Novel green fluorescent polyamines to analyze ATP13A2 and ATP13A3 activity in the mammalian polyamine transport system

Marine Houdou[1,2,†], Nathalie Jacobs[1,†], Jonathan Coene[3,†], Mujahid Azfar[1], Roeland Vanhoutte[3], Chris Van den Haute[2,4,5], Jan Eggermont[1], Veronique Daniëls[2,5], Steven H. L. Verhelst[3,‡,*] and Peter Vangheluwe[1,2,‡,*].

[1] Laboratory of Cellular Transport Systems, Department of Cellular and Molecular Medicine, KU Leuven, B-3000 Leuven, Belgium

[2] Aligning Science Across Parkinson's (ASAP) Collaborative Research Network, KU Leuven, B-3000 Leuven, Belgium

[3] Laboratory of Chemical Biology, Department of Cellular and Molecular Medicine, KU Leuven, B-3000 Leuven, Belgium

[4] Leuven Viral Vector Core, KU Leuven, Leuven, Belgium.

[5] Research Group for Neurobiology and Gene Therapy, Department of Neurosciences, KU Leuven, B-3000 Leuven, Belgium

†, ‡ These authors contributed equally to this work.

* Correspondence: steven.verhelst@kuleuven.be; +32 16 37 45 17; SV and peter.vangheluwe@kuleuven.be; +32 16 33 07 20; PV.

Abstract: Cells acquire the polyamines putrescine (PUT), spermidine (SPD) and spermine (SPM) *via* the complementary action of polyamine uptake and synthesis pathways. The endosomal P_{5B}-type ATPases ATP13A2 and ATP13A3 emerge as major determinants of mammalian polyamine uptake. Our biochemical evidence shows that fluorescently labeled polyamines are genuine substrates of ATP13A2. They can be used to measure polyamine uptake in ATP13A2 and ATP13A3-dependent cell models resembling radiolabeled polyamine uptake. We further report that ATP13A3 enables faster and stronger cellular polyamine uptake than ATP13A2. We also compared the uptake of new green-fluorescent PUT, SPD and SPM analogs using different coupling strategies (amide, triazole or isothiocyanate) and fluorophores (symmetrical BODIPY, BODIPY-FL and FITC). ATP13A2 promotes the uptake of various SPD and SPM analogs, whereas ATP13A3 mainly stimulates the uptake of PUT and SPD conjugates. However, the polyamine linker and coupling position on the fluorophore impacts the transport capacity, whereas replacing the fluorophore affects polyamine selectivity. The highest uptake in ATP13A2 or ATP13A3 cells is observed with BODIPY-FL-amide conjugated to SPD, whereas BODIPY-PUT analogs are specifically taken up *via* ATP13A3. We found that P_{5B}-type ATPase isoforms transport fluorescently labeled polyamine analogs with a distinct structure-activity relationship (SAR) suggesting that isoform-specific polyamine probes can be designed.

Keywords: Fluorescently labeled polyamines, mammalian polyamine transport systems, P_{5B}-type ATPases, radiolabeled polyamines.

Introduction

Polyamines such as putrescine (PUT), spermidine (SPD) and spermine (SPM) are ubiquitous and physiologically important organic polycations found in every living cell. Polyamines are implicated in a broad range of cellular processes, ranging from cell proliferation to signaling, but their levels decline with aging [1,2]. Conversely, polyamine supplementation increases lifespan of model organisms such as mice and fruit fly [3,4]. At the molecular level, polyamine biosynthesis and catabolism pathways are well understood, but a clear knowledge gap remains regarding the molecular characteristics of the mammalian polyamine transport systems (mPTS). Three main mechanisms have been proposed to be involved in cellular polyamine uptake [5]: (i) a direct transport at the plasma membrane, (ii) a glypican-mediated uptake *via* endocytosis and (iii) a caveolin-1-mediated endocytosis [5-10]. Recently, we identified two key players of the mPTS that belong to the P_{5B}-type ATPases (ATP13A2 and ATP13A3) [11-13].

In humans, ATP13A2 and ATP13A3 are ubiquitously expressed with highest expression in the brain and the liver, respectively ([14] and https://www.proteinatlas.org). At the subcellular level, both proteins are localized in the endosomal pathway with a preferred late endo-/lysosomal distribution for ATP13A2 [12-14] and early/recycling endosomes for ATP13A3 [12,13,15]. We provided biochemical evidence that human ATP13A2 (hATP13A2) transports polyamines from late endo/lysosomes to the cytosol with a high affinity for SPM and SPD [13], which was confirmed at the structural level [16-20]. ATP13A2, and also the closely related ATP13A3, fulfill their polyamine transport function downstream of polyamine internalization *via* endocytosis [11,13]. Both transporters are implicated in disease, since genetic mutations in *ATP13A2* have been linked to neurodegeneration, whereas ATP13A3 is genetically implicated in pulmonary arterial hypertension and may play a role in cancer (see [14] and references therein). Studying the transporters of the mPTS in cells typically relies on the use of radiolabeled (^{3}H and/or ^{14}C) or fluorescently labeled polyamines. We recently reported fluorescent polyamine conjugates incorporating a symmetrical BODIPY fluorophore (referred to as 'BODIPY' throughout the manuscript). These have proven invaluable to characterize the P_{5B}-type ATPases [11,21]. Indeed, ATP13A2 contributes to the cellular uptake of BODIPY-SPM and BODIPY-SPD in human neuroblastoma (SH-SY5Y) cells [13] corresponding to the substrate specificity of purified ATP13A2

for SPM and SPD [13]. We further demonstrated that ATP13A3 is responsible for the impaired BODIPY-PUT uptake observed in the CHO-MG cell line with a deficient mPTS [11,22].

Despite their proven value, it remains unclear how the transport of these polyamine conjugates compares with unlabeled polyamines and whether the fluorophore or its linkage to the polyamine may influence the recognition and transport by the P_{5B}-type ATPases. Here, we report our recent work aimed at addressing these questions. Specifically, we compared uptake of BODIPY- and ^{14}C-labeled polyamines in two cell models relying either on ATP13A2 or ATP13A3 activity. Additionally, with a series of new green fluorescent analogs of PUT, SPD and SPM we tested the impact of different coupling strategies and fluorescent headgroups on transport capacities. Interestingly, we found that a broad range of fluorescent polyamine probes are taken up in cells *via* the catalytic activity of ATP13A2 and/or ATP13A3, although probe- and isoform-specific effects are observed. Overall, this work provides novel fluorescent polyamine conjugates with improved properties for the study of P_{5B}-type ATPases in disease models, and opens the way for the design of P_{5B} isoform-specific polyamine probes.

Materials and Methods

Preparation of compounds

All fluorescent polyamine probes were prepared in a final stock concentration of 5 mM in 0.1 M γ-(N-Morpholino) propanesulfonic acid (MOPS; PanReac AppliChem, A1076,1000), brought to pH 7.0 with KOH (Honeywell, 319376 Fluka) and stored at -20°C. Unclicked SPM-N_3-4·HCl (azide SPM) was dissolved in MOPS-KOH to reach 20 mM, unclicked BODIPY-alkyne was dissolved in dimethyl sulfoxide (DMSO; Sigma, D5879) to a final concentration of 5 mM and they were both stored at -20°C. Unlabeled polyamines, putrescine dihydrochloride (PUT; Sigma: P7505), spermidine (SPD; Sigma: S2626) and spermine (SPM; Sigma: 85590) were dissolved in MOPS-KOH (pH 7.0) at a final concentration of 500 mM (putrescine and spermidine) or 200 mM (spermine) and stored at -80 °C.

For the biochemical ATP/NADH-enzyme coupled ATPase assay, the following stock solutions were prepared: 2.5 M potassium chloride (KCl; Sigma: P5405), 1 M magnesium chloride solution ($MgCl_2$; Gibco: M1028), 15.625 U/µL lactate dehydrogenase (Sigma: L2500) and 4 U/µL pyruvate kinase (Sigma: P1506), and were stored at 4 °C. Additionally, 100 mM β-nicotinamide adenine dinucleotide reduced disodium salt hydrate (NADH; Sigma: 43420) in MOPS-KOH (pH 7.0), 50 mM phospho(enol)pyruvic acid tri(cyclohexylammonium) salt (PEP; Sigma: P7252), 500 mM dithiothreitol (DTT; PanReac AppliChem: A2948.0025), and 63 mM adenosine 5'-triphosphate disodium salt trihydrate brought to pH 7.0 (Roche: ATPD-RO), were stored at -20°C.

For the preparation of HMEC-1 cell culture medium, a 100 µg/mL stock of human epidermal growth factor (hEGF; Sigma: E9644) was prepared in 0.22 µm filter-sterilized 10 mM acetic acid (Chem Lab: CL00.0119.1000), supplemented with 1% albumin fraction V (Carl Roth: 8076.4), in Milli-Q, and was stored at -80°C in aliquots. Additionally, hydrocortisone (Sigma: H0888) was dissolved in absolute ethanol (VWR Chemicals: 20821.296) and diluted 1:25 in MCDB131 medium to a final concentration of 100 µg/mL, and stored in aliquots at -20°C.

The endocytosis inhibitors Dynasore (Sigma: D7693), Genistein (Abcam: ab120112), and Pitstop-2 (Sigma: SML1169) were dissolved in DMSO to a final stock concentration of 50 mM, 25 mM and 25 mM, respectively, and stored at -20°C.

Lentiviral transduction and cell culture

SH-SY5Y human immortalized neuroblastoma cells (ATCC: CRL-2266™, Lot Number 62431864) were transduced with lentiviral vectors to obtain stable overexpression of human ATP13A2 (isoform 2, wild-type (ID: NP_001135445) or catalytically dead mutant, D508N) [13]. Lentiviral vectors were produced by the Leuven Viral Vector Core using pLenti HsATP13A2 WT (Addgene plasmid #171485; http://n2t.net/addgene:171485; RRID: Addgene_171485) as described in dx.doi.org/10.17504/protocols.io.bw57pg9n. SH-SY5Y cells were cultured in DMEM high glucose culture medium (Gibco: 41965), supplemented with 1% MEM Non-Essential Amino Acid Solution (Merck: M7145), 1 mM sodium pyruvate (Gibco: 11360070), 1% Penicillin-Streptomycin (Sigma: P4458), and 15% heat-inactivated Fetal Bovine Serum Standard, South America origin (FBS; PAN BioTech: P30-3306) at 37 °C with 5% CO_2. After lentiviral transduction, cells were selected with 2 µg/mL puromycin (Invivogen: ant-pr-1).

HMEC-1 human immortalized microvascular endothelial cells (ATCC: CRL-3243™, Lot Number: 70022309) were transduced with lentiviral vectors to obtain stable overexpression of human ATP13A3 (wild type or catalytically dead mutant, D498N). HMEC-1 cells were cultured in 0.2% gelatin (Sigma, G1393) coated 75 cm^2 flasks and in MCDB131 culture medium without L-glutamine (Gibco: 10372-019), supplemented with 10 ng mL-1 hEGF, 1 µg mL-1 Hydrocortisone, 10 mM GlutaMAX supplement (Gibco: 35050061), 1% Penicillin-Streptomycin and 10% heat-inactivated Fetal Bovine Serum Standard, South America origin at 37 °C with 5% CO_2. After lentiviral transduction, cells were selected with 1 µg/mL puromycin.

All cell lines were routinely tested for mycoplasma contamination using the PlasmoTest Mycoplasma detection kit (Invivogen: rep-pt1).

Western blotting

Cells were detached either by scrapping them in Dulbecco's phosphate buffered saline modified without calcium chloride and magnesium chloride (DPBS; Gibco: D8537) (SH-SY5Y) or, using 0.25% Trypsin-EDTA (Gibco: 25200056) (HMEC-1) for which the enzymatic reaction was stopped by addition of culture medium. Cell suspensions were centrifuged at 4°C for 5 minutes at 450 g (SH-SY5Y) and 2500

rpm (HMEC-1). Cell pellets were washed twice with DPBS and centrifuged again before being lysed in RIPA buffer (RIPA lysis and extraction buffer (Invitrogen: 89900) supplemented with protease cocktail inhibitors (SIGMAFAST Protease Inhibitor Cocktail Tablets, EDTA-Free (Sigma: S8830)). Lysis was done on ice for 30 minutes and a further centrifugation at 4°C for 30 minutes at 20,000 g. Supernatants were kept and protein concentration was estimated using the micro-BCA Protein Assay Kit (Pierce BCA Protein Assay Kit (Thermo Scientific: 23225)). 20 µg of protein were mixed with NuPAGE LDS sample buffer (Invitrogen: NP0007) with 5% β-mercaptoethanol. Samples were not boiled, separated on 4-12% Bis-Tris gels (Invitrogen: NP0321BOX) and transferred onto PVDF membranes (Thermo Scientific: 88518) using a liquid transfer (1h15, 100V, 4°C). Membranes were then blocked in blocking buffer (5% milk powder in 1X TBS and 0.1% Tween20) for 1 h at room temperature, then incubated overnight at 4°C with the primary antibodies 1% bovine serum albumin in 1X TBS-Tween20 (TBS-T) buffer and washed three times for 5 min in TBS-T. Membranes were then incubated with peroxidase-conjugated secondary goat anti-rabbit or goat anti-mouse antibodies in 1% milk powder in 1X TBS-T buffer for 1 h at room temperature and later washed five times for 5 min in TBS-T. Signal was detected with chemiluminescence reagent (SuperSignal West Pico PLUS chemiluminescent Substrate, Thermo Scientific: 34095) using a Biorad camera (Vilber Lourmat) and its software (ImageLab). This specific protocol for ATP13A2 and ATP13A3 western blotting is also described in protocols.io (dx.doi.org/10.17504/protocols.io.81wgbyzqovpk/v1).

Mouse monoclonal anti-GAPDH (G8795, lot #067M4785V, dilution 1:5,000), and rabbit anti-ATP13A2 antibodies (A3361, lot #0000102992, dilution 1:1,000) were purchased from Sigma. Goat anti-rabbit IgG (H+L) secondary antibody HRP conjugated (31460) and goat anti-mouse IgG (H+L) secondary antibody HRP conjugated (31430) were from Thermo Scientific and rabbit anti-ATP13A3 antibody (HPA029471, lot # 000035781, dilution 1:2,000) was from Atlas Antibodies.

ATP/NADH-enzyme coupled ATPase assay.

Purified human ATP13A2 protein was obtained as previously described in [13]. Protein concentration was determined using a Pierce 660 nm Protein Assay (Thermo Scientific: 22660) and the quality of the purification was assessed via SDS-PAGE followed by InstantBlue Coomassie protein stain (abcam: ab119211) staining and immunoblotting, as described in [11]. To measure ATPase activation of purified

ATP13A2, serial dilutions of the unlabeled, unclicked azide spermine, BODIPY-SPM, and unclicked alkyne BODIPY were prepared ranging from 0.01 µM to 10 mM, in a final volume of 25 µL per well in a 384-well clear polystyrene microplate. Then, 40 µL of the reagent mix containing 50 mM MOPS-KOH (pH 7.0), 100 mM KCl, 30 mM $MgCl_2$, 0.6 mM NADH, 1.667 mM PEP, 2.4 U µL-1 pyruvate kinase, 2.4 U µL-1 lactate dehydrogenase, and 2 mM DTT, in the presence or absence of 1.25 µg purified ATP13A2 protein, were added per well. Next, 5 mM ATP (pH 7.0) were added in each well to start the biochemical reaction. The plate was shaken for 30 seconds prior acquisition. Absorbance at 340 nm was measured at RT every 30 seconds for 1 h with a SpectraMax Plus 384 microplate reader (Molecular Devices). Data analysis was done using SoftMax Pro 7.0 and GraphPad Prism 9.3.1 software. This protocol is further described in protocols.io following dx.doi.org/10.17504/protocols.io.6qpvr4do2gmk/v1.

Chemical synthesis of fluorescently labeled polyamines

The detailed synthesis of each compound is further described in **Supplementary Information, Figures S5-8.**

Acquisition of absorption and emission spectra

Absorbance spectra were determined using the Cary 60 UV-Vis spectrophotometer with 1 nm spectral resolution. Attenuators were used to remove the effect of background and noise. Emission spectra were measured using an Edinburgh Instruments FLS 980 spectrometer at an excitation wavelength of 465 nm and emission data was collected at 1 nm intervals. For both emission and absorbance measurements, probe samples were dissolved in deionized water as to keep the optical density below 0.2. After this the samples were added to a quartz cuvette with 10 mm pathlength before being sealed and measured.

Cellular polyamine uptake and endocytosis assay.

Cells were seeded in 12-well plates to reach 70% confluency the day of the experiment (approximately 2.0 x 10^5 and 1.5 x 10^5 cells per well, for SH-SY5Y and HMEC-1, respectively). To assess the polyamine uptake capacity, cells were incubated with 0.1 µM to 100 µM of fluorescently labeled polyamines in their respective medium for 0 to 16 h at 37°C and 5% CO_2. To assess endocytosis rate, cells were treated with a cocktail of endocytosis inhibitors containing 100 µM Dynasore, 50 µM Genistein, and 50 µM

Pitstop-2, dissolved in their respective culturing medium without supplementation of FBS, for 30 min at 37°C and 5% CO_2, and kept at 4°C for 15 min. Then, cells were co-incubated with 50 µg/mL Alexa647-Transferrin (Invitrogen: T23366) for 20 min at 4°C, and further incubated for 20 min at 37°C and 5% CO_2. After either treatment, cells were washed with DPBS or Versene Solution (Gibco: 15040), detached with either TryplE or 0.25% Trypsin-EDTA, centrifuged and resuspended in DPBS containing 1% Albumin Fraction V. Cell suspensions were filtered through a nylon filter to avoid clumps and kept on ice before acquisition using a BD FACS Canto II AIG or HTS Flow Cytometer (BD Biosciences). A 488 nm 20 mW Solid State Blue (Coherent) laser with 530/30 BP detector, and a 633 nm 17 mW HeNe Red (JDS Uniphase) laser with 660/20 detector were used to record the mean fluorescent intensities (MFI) of 10,000 events per sample. These protocols are described in protocols.io following dx.doi.org/10.17504/protocols.io.n92ldp8qxl5b/v1 and dx.doi.org/10.17504/protocols.io.8epv5jjedl1b/v1, respectively. Data analysis was done using Flowing Software 2 and GraphPad Prism 9.3.1.

Radiolabeled polyamine uptake assay.

Cells were seeded in 12-well plates to reach 70% confluency the day of the experiment. Cells were incubated with 0.5 to 5 µM of [^{14}C]-radiolabeled polyamines ([^{14}C]-PUT: ARC 0245-50 µCi; [^{14}C]-SPD: ARC 3138-50 µCi; and [^{14}C]-SPM: ARC 3139-50 µCi) in culture medium for 30 min at 37°C. Afterwards, cells were washed with cold DPBS, supplemented with 50 µM of the respective unlabeled polyamine. After two washing steps with cold DPBS, the cells were lysed using 0.1% SDS (Sigma, 71725) in DPBS. After 10 min, the cell lysates were scraped off the wells and collected into scintillation vials containing 7 mL EcoLite Liquid Scintillation Cocktail (MP Biomedicals: 01882475-CF). [^{14}C] radioactivity in counts-per-minute (CPM) was measured by liquid scintillation counting (TRI-CARB 4910TR V Liquid Scintillation Counter, PerkinElmer). This protocol is further described in protocols.io following dx.doi.org/10.17504/protocols.io.yxmvm2x85g3p/v1.

Statistics and data analysis.

Experiments on the different cell models were executed by different researchers, which provided consistent results that independently confirmed the major conclusions. Data are expressed as the mean ± SD, or with individual data points (replicates of multiple independent experiments). GraphPad Prism

9.3.1 software was used to plot all graphs and to perform all of the required statistical assessments. Statistical tests for each graph are described in the legend together with the number of independent biological experiments. For the quantification of immunoblots, ImageJ was used.

Results

1. BODIPY-conjugated SPM is a genuine transport substrate of ATP13A2

hATP13A2 exhibits the highest affinity for SPM [13], which binds to a narrow channel-like substrate binding site at the luminal side of the protein [16-20]. Whether the polyamine pocket may also accommodate the bulkier BODIPY-SPM for subsequent transport remains unclear. Since SPM transport by ATP13A2 is coupled to the hydrolysis of ATP, we examined whether BODIPY-SPM also stimulates ATP turnover, and hence represents a genuine substrate. To this end, we purified human WT ATP13A2 (**Figure 1A, B**) and performed an ATP/NADH enzyme-coupled ATPase assay with SPM or BODIPY-SPM (**Figure 1C**). ATP13A2's ATPase activity is stimulated with either SPM, BODIPY-SPM or clickable azide SPM (an intermediate in the coupling strategy), but not with clickable BODIPY-alkyne (**Figure 1C**). Hence, ATP13A2 recognizes the BODIPY-labeled or clickable SPM as genuine substrates. Surprisingly, ATP13A2 displays a higher apparent affinity, and slightly lower maximal velocity (V_{max}), for BODIPY-SPM (K_m 0.22 µM) than SPM (K_m 79 µM).

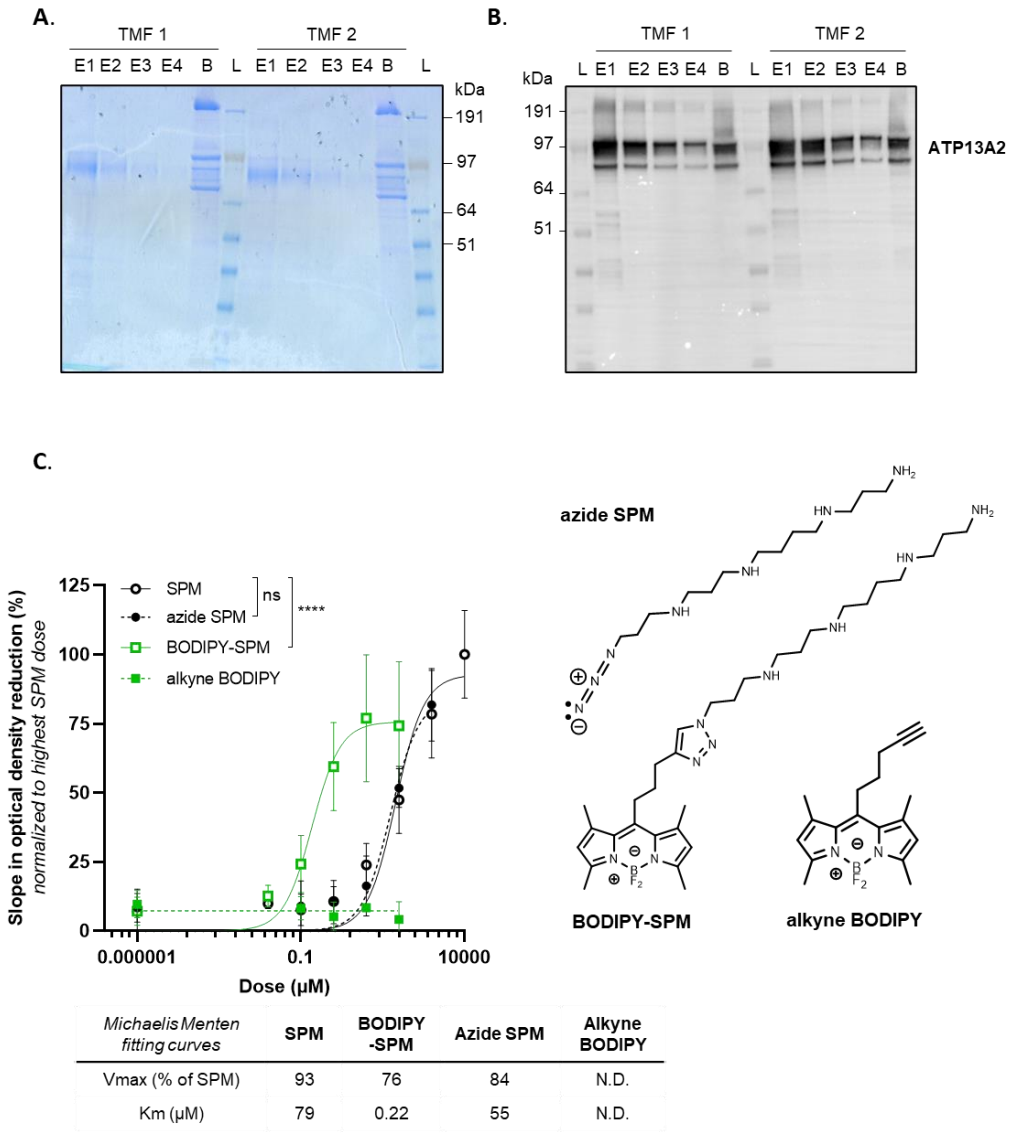

Michaelis Menten fitting curves	SPM	BODIPY -SPM	Azide SPM	Alkyne BODIPY
Vmax (% of SPM)	93	76	84	N.D.
Km (µM)	79	0.22	55	N.D.

Figure 1. **Purification and ATPase activity of hATP13A2. A**. Coomassie staining showing the purified human ATP13A2 protein present in the different elution fractions (E1 to E4) from total membrane fraction (TMF) and onto the beads (B). **B.** Immunoblot analysis of ATP13A2 purified protein from the fractions depicted in **A**. **C**. ATPase activity of purified ATP13A2 (1.25 µg) measured with increasing concentrations of unlabeled spermine (SPM), clickable spermine (azide SPM), free BODIPY (alkyne BODIPY) and BODIPY-SPM, which structures are presented on the right (N = 2 to 7, technical duplicates, two-way ANOVA with Tukey's multiple comparisons test). The Y axis depicts the slope in optical density at 340 nm reflecting NADH consumption and further ATP consumption, normalized to the highest dose of SPM. N.D., not determined.

We previously studied ATP13A2-dependent BODIPY-SPM uptake in human neuroblastoma SH-SY5Y cells, a frequently used cell line in Parkinson's disease research [13,23]. Here, we characterized the time- and dose-dependency of BODIPY-SPM uptake in SH-SY5Y cells overexpressing ATP13A2 wild type (A2 WT-OE) or a transport-dead mutant (D508N-OE). Both cell models exhibit comparable

ATP13A2 protein expression levels (**Figure S1A**) and interestingly, a significantly higher endocytosis rate in A2 D508N-OE cells compared with A2 WT-OE and NTS cells (**Figure S1B**), suggesting that the difference in BODIPY-SPM uptake between A2 WT-OE and A2 D508N-OE cells can be attributed to ATP13A2 transport activity. The time-dependency was evaluated by incubating the cells with 5 µM BODIPY-SPM (a concentration that was used before; [13]) up to 16 h (**Figure S1C).** The maximal fold difference in BODIPY-SPM uptake between A2 WT-OE and A2 D508N-OE cells was reached at 4 h (1.6-fold) **(Figure S1C**), whereas maximal cellular uptake capacities were still not achieved at 16 h (**Figure S1C**). We selected a 2 h incubation time, which falls within the linear phase of the BODIPY-SPM uptake (**Figure 2A**), to examine the dose-dependency of BODIPY-SPM uptake in ATP13A2 cell models (**Figure 2B** and **Figure S1C**). We observed a 5-fold higher BODIPY-SPM uptake in A2 WT-OE *versus* A2 D508N-OE cells at the lowest BODIPY-SPM concentration (0.1 µM, **Figure S1D**), but the fold difference decreases at higher concentrations. Nevertheless, a significant and reproducible 1.6-fold higher uptake was observed at 5 µM BODIPY-SPM (**Figure 2C**), which was used in previous studies [13]. Finally, we compared BODIPY-SPM with radiolabeled spermine (^{14}C-SPM) uptake in A2 WT-OE cells to assess the impact of the fluorescent tag on cellular uptake capacities (**Figure 2D**). After incubating A2 WT-OE and D508N-OE cells for 30 min with either 5 µM of BODIPY-SPM or ^{14}C-SPM, we observed a significant 1.33-fold higher uptake for ^{14}C-SPM (**Figure 2D**). The effect of the fluorescent tag on SPM uptake reflects the higher apparent affinity, but lower V_{max} of ATP13A2 for BODIPY-labeled *versus* native spermine (**Figure 1C**). Overall, our data demonstrate that the BODIPY-SPM probe is a valuable tool to evaluate the ATP13A2 transport activity in cells.

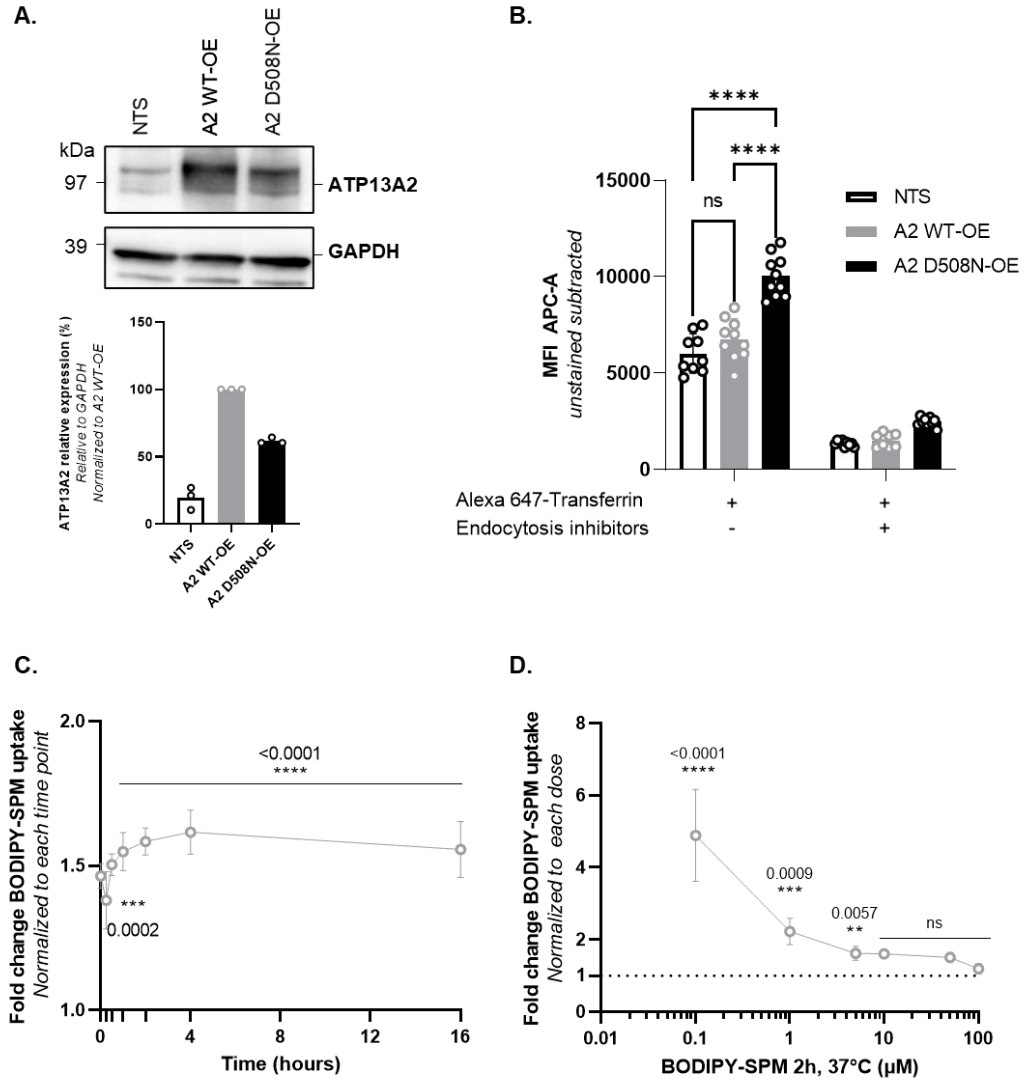

Figure S1. Characterization of ATP13A2-expressing SH-SY5Y cell models. A. ATP13A2 protein expression level in SH-SY5Y cells transduced with lentiviral particles to overexpress ATP13A2 wild type (A2 WT-OE) or the catalytically dead mutant ATP13A2 D508N (A2 D508N-OE). Immunoblots showing ATP13A2 expression levels and quantification (bar graph) relative to GAPDH signal (N=3). **B.** The endocytosis rate in the ATP13A2 cell models was assessed by an Alexa 647-transferrin assay. A2 WT-OE, A2 D508N-OE and non-transduced (NTS) cells were incubated with Alexa 647-transferrin in the presence or absence of a cocktail of endocytosis inhibitors: dynasore (100 µM), genistein (50 µM) and pitstop-2 (50 µM). The mean fluorescence intensity (MFI) of 10,000 events was recorded on the Canto II HTS flow cytometer (N=3, two to four technical replicates, two-way ANOVA with Tukey's multiple comparisons test). In both panels (**A** and **B**), the NTS cell line was used as a control. **C**. and **D**. Graph depicts the fold change in BODIPY-SPM uptake between A2 WT-OE and A2 D508N-OE cells, normalized to each time point considered (**C**) or each dose considered (**D**) (N=3 to 10, technical duplicates, two-way ANOVA with Sidak's multiple comparisons test).

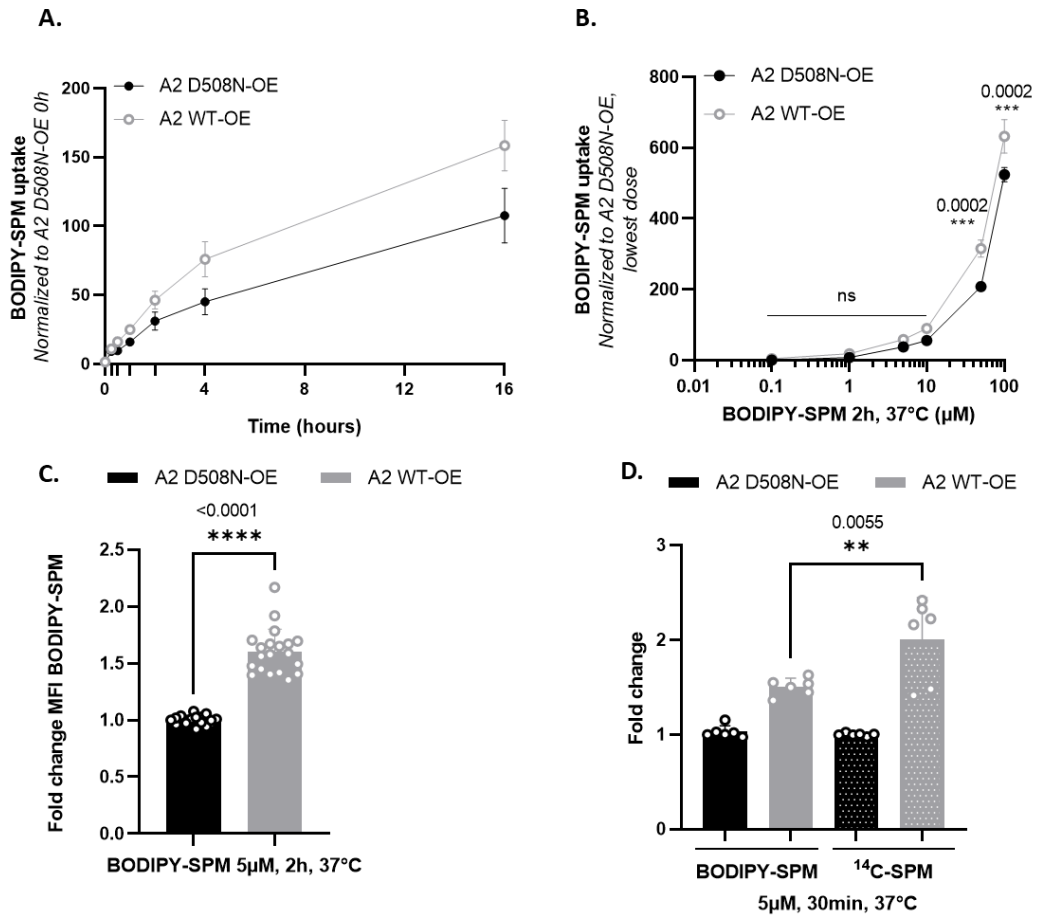

Figure 2. Time- and dose-dependency of BODIPY-SPM uptake in ATP13A2-expressing SH-SY5Y cell models. A-B. SH-SY5Y cells were incubated with 5 µM BODIPY-SPM for the indicated times (**A**, time dependency) or with increasing concentrations of BODIPY-SPM for 2 h (**B**, dose dependency). The mean fluorescence intensity (MFI) of 10,000 events was recorded using a BD Canto II HTS flow cytometer. Graphs represent the MFI recorded in ATP13A2 WT OE (A2 WT-OE) and ATP13A2 D508N-OE (A2 D508N-OE) cells, normalized to the 0 h incubation time in A2 D508N-OE cells (in **A**) or to the lowest concentration of BODIPY-SPM (*i.e.* 100 µM) in A2 D508N-OE cells (in **B**). **C.** Graph depicts the fold change in BODIPY-SPM uptake (5 µM; 2 h) between A2 WT-OE and A2 D508N-OE cells (N=10, technical duplicates, unpaired t-test). **D.** Comparison of the uptake of 5µM BODIPY-conjugated (BDP-SPM) *versus* 5 µM radiolabeled spermine (^{14}C-SPM) in SH-SY5Y A2 WT-OE and D508N-OE cells for 30 minutes (N=3, technical duplicates, one-way ANOVA with Tukey's multiple comparisons test).

2. Evaluation of BODIPY-PUT and BODIPY-SPD uptake in a new human ATP13A3 cell model.

Besides ATP13A2, we previously reported that ATP13A3 also modulates cellular BODIPY-polyamine uptake in CHO cells, with the strongest impact on BODIPY-PUT uptake [11]. Here, we decided to evaluate the uptake of the BODIPY-PUT and BODIPY-SPD probes in the context of human ATP13A3, and turned to immortalized human dermal microvascular endothelial cells (HMEC-1). HMEC-1 cells are frequently used in the context of pulmonary arterial hypertension, a disease that is associated with ATP13A3 mutations [24-27] and do express ATP13A3. We generated HMEC-1 cells with stable lentiviral mediated over-expression of ATP13A3 WT (A3 WT-OE) or a catalytic dead mutant D498N (A3 D498N-OE), and confirmed that both the ATP13A3 expression level (**Figure S2A**) and endocytosis rate (**Figure S2B**) of A3 WT-OE and A3 D498N-OE HMEC-1 cells were comparable. Hence, differences in BODIPY-polyamine uptake between A3 WT-OE and A3 D498N-OE cells can be attributed to a functional involvement of the transport ATPase.

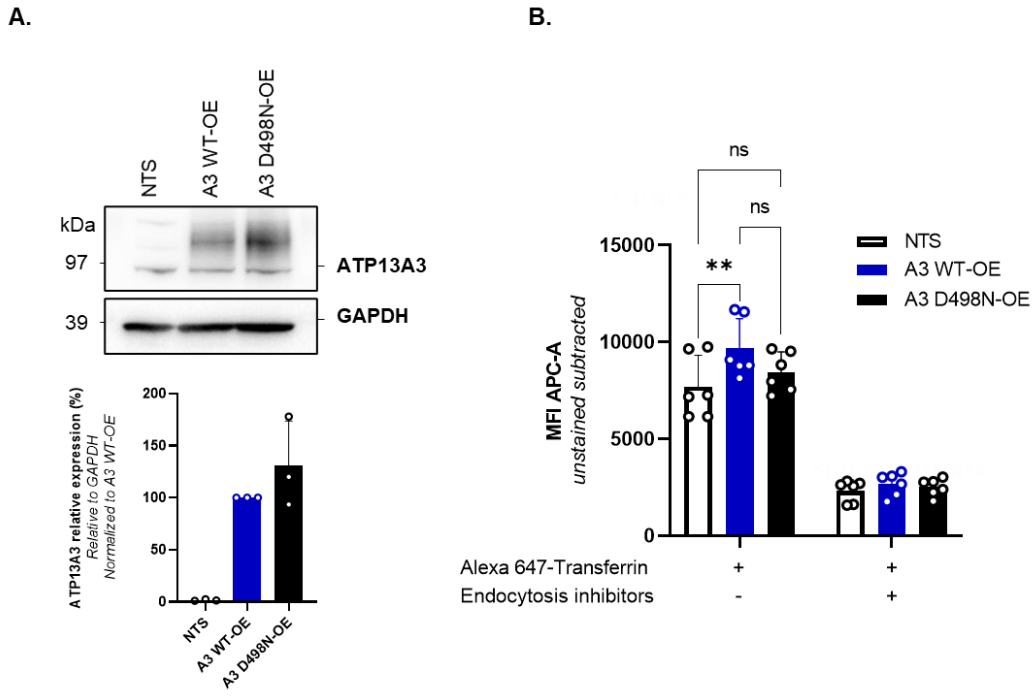

Figure S2. Characterization of ATP13A3-expressing HMEC-1 cell models. A. HMEC-1 cells were transduced with lentiviral particles to overexpress ATP13A3 wild type (A3 WT-OE) or the catalytically dead mutant ATP13A3 D498N (A3 D498N-OE). Immunoblots showing ATP13A3 expression levels and quantification (bar graph) relative to GAPDH signal (N=3). **B**. Evaluation of the endocytosis rate in A3 WT-OE and A3 D498N-OE HMEC-1 cells. Cells were incubated with Alexa 647-transferrin in the presence or absence of a cocktail of

endocytosis inhibitors: dynasore (100 µM), genistein (50 µM) and pitstop-2 (50 µM). The mean fluorescence intensity (MFI) of 10,000 events was recorded on the Canto II HTS flow cytometer . N=3 with technical duplicates, two-way ANOVA with Tukey's multiple comparisons test. In both panels, the non-transduced cell line (NTS) was used as a control.

Next, we analyzed the time- and dose-dependency of BODIPY-SPD and BODIPY-PUT uptake in the ATP13A3 cell models (**Figure 3** and **Figure S3**). First, we evaluated the ATP13A3-dependent BODIPY-PUT and BODIPY-SPD uptake (5µM) in HMEC-1 over time (**Figure S3A**, **C** and **Figure 3A**, **C**). At 4 h, the cellular uptake of both probes reached saturation. Interestingly, at 5 µM BODIPY-polyamine, A3 WT-OE cells exhibit a more pronounced uptake than A2 WT-OE cells, already at early time points. Therefore, a shorter incubation time of 30 min is required to remain in the linear uptake phase in A3 WT-OE cells (**Figure 3A, C**) in comparison to the 2 h incubation in A2 WT-OE cells (**Figure 2A**). This may reflect the differences in (i) endosomal localization between ATP13A3 (early/recycling endosomes) and ATP13A2 (late endo/lysosomes) [11-13], (ii) cell type properties (endothelial versus neuroblastoma cells) and/or (iii) relative expression levels of ATP13A3 *versus* ATP13A2.

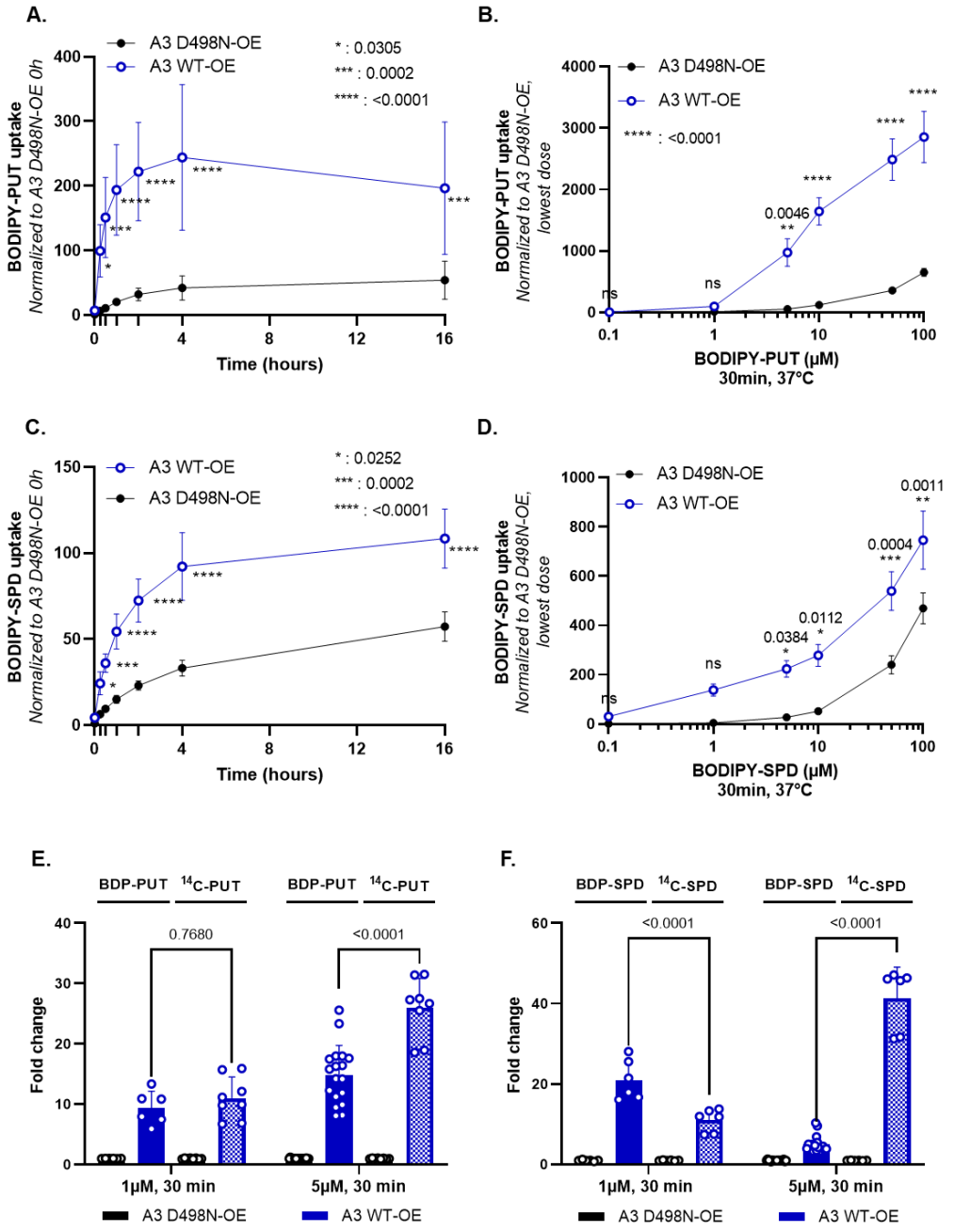

Figure 3. Time- and dose-dependency of BODIPY-PUT and BODIPY-SPD uptake in ATP13A3-expressing HMEC-1 cell models. A. and **C**. Time dependent BODIPY-polyamine uptake in HMEC-1 cells incubated with 5 µM BODIPY-PUT (**A**) or BODIPY-SPD (**C**). The mean fluorescence intensity (MFI) of 10,000 events was recorded using a BD Canto II HTS flow cytometer. Graphs represent the fold change between the MFI recorded in A3 WT-OE *versus* A3 D498N-OE cells, normalized to the 0 h incubation time in A3 D498N-OE cells. (N=3 to 9, with technical duplicates, two-way ANOVA with Sidak's multiple comparisons test **B**. and **D**. Dose-response of BODIPY-PUT (**B**) or BODIPY-SPD (**D**) uptake in HMEC-1 cells at 30 minThe MFI of 10,000 events was recorded using a BD Canto II HTS flow cytometer. Graphs represent the fold change difference between the MFI recorded in A3 WT-OE and A3 D498N-OE cells, normalized to the highest concentration of BODIPY-polyamine (i.e. 100 µM) in A3 D498N-OE cells (N=3 to 9, with technical duplicates, two-way ANOVA with Sidak's multiple comparison test). **E**. and **F**. Comparison of the uptake of 1 and 5 µM BODIPY-conjugated (BDP-PUT and BDP-

SPD) *versus* radiolabeled putrescine and spermidine (^{14}C-PUT and ^{14}C-SPD) in HMEC-1 A3 WT-OE and D498N-OE cells for 30 min (N=3 to 9, technical duplicates, two-way ANOVA with Tukey's multiple comparisons test).

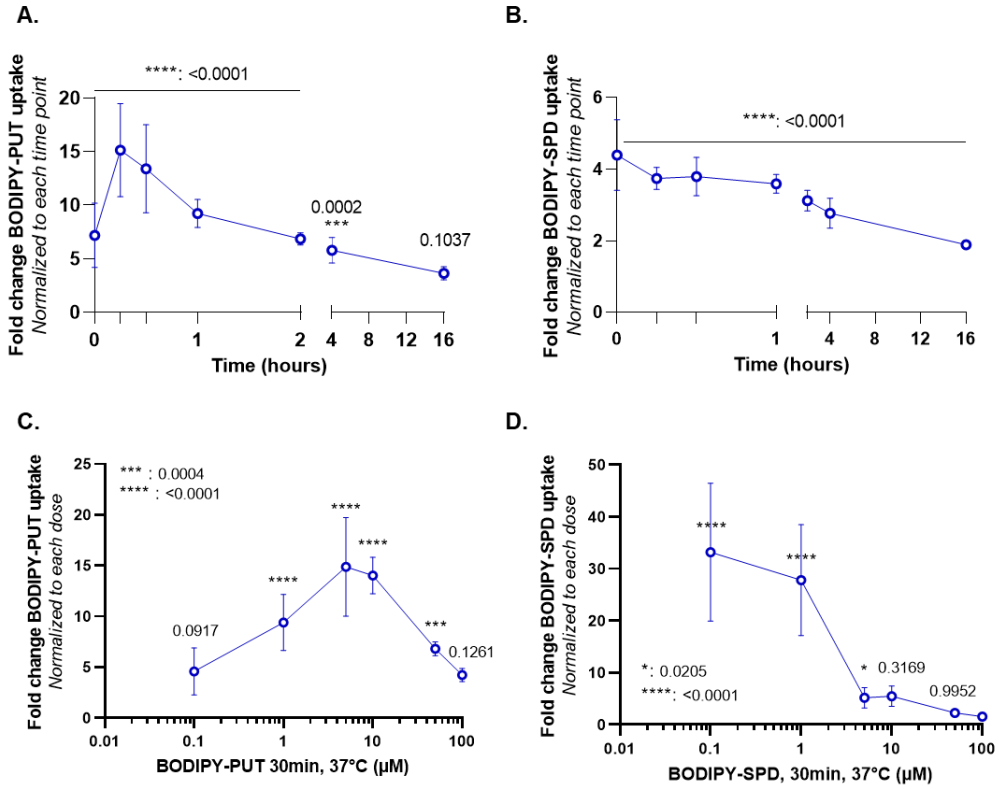

Figure S3. BODIPY-PUT and BODIPY-SPD uptake in HMEC-1 cells overexpressing ATP13A3 WT or D498N. Fold change in BODIPY-PUT (**A**, **C**) and BODIPY-SPD (**B**, **D**) uptake between A3 WT-OE and A3 D498N-OE cells, normalized to each time point considered (**A**, **B**) or each dose considered (**C**, **D**). N=3 to 9, technical duplicates, two-way ANOVA with Sidak's multiple comparisons test.

Second, we performed a dose-response experiment with increasing concentrations of BODIPY-PUT or -SPD (0 - 100 µM) after 30 min incubation (**Figure 3B, D**). At 1 µM, ATP13A3-mediated BODIPY-SPD uptake is more pronounced than BODIPY-PUT, indicating that ATP13A3 may present a higher apparent affinity and/or V_{max} for BODIPY-SPD. A higher maximal fold increase is also observed with BODIPY-SPD (33-fold at 0.1 µM, **Figure S3D**) than for BODIPY-PUT (15-fold at 5 µM, **Figure S3C**). The higher fold uptake with 5 µM ^{14}C-SPD (41-fold) (**Figure** 3E) than with 5 µM ^{14}C-PUT (26-fold) (**Figure 3F**) indicates that ATP13A3 presents a higher transport activity with SPD than with PUT. To investigate the impact of the fluorescent headgroup, we compared the uptake of BODIPY-labeled with ^{14}C-radiolabeled SPD and PUT in A3 WT-OE cells at two different concentrations (1 µM and 5 µM) (**Figure 3D, E**). At 1 µM, a comparable fold change in uptake can be observed between BODIPY-PUT

(9.4-fold) *versus* ^{14}C-PUT (11-fold), whereas the uptake of BODIPY-SPD is significantly higher (21-fold) than ^{14}C-SPD (11.6-fold). At 5 µM, the uptake of the BODIPY probes is lower compared with ^{14}C-labeled polyamines, especially for BODIPY-SPD. Our results therefore suggest that ATP13A3 presents a higher apparent affinity and/or reduced maximal uptake activity towards BODIPY- as compared to ^{14}C-labeled probes, similar to what we have observed for ATP13A2.

3. Chemical synthesis of novel green fluorescent polyamine conjugates.

Our results so far demonstrated that both radiolabeled and BODIPY-polyamines are taken up in cells *via* ATP13A2 and ATP13A3. Next, we explored whether the coupling strategy or the headgroup fluorophore of the fluorescent conjugates may influence the transport by ATP13A2 and/or ATP13A3 (**Figure 4**). The synthesis of the click-chemistry derived BODIPY-conjugated polyamines (**compounds 1a-c** in **Figure 4**) was performed as previously described [11,21] with small modifications indicated in **Supplementary Information**. Here, we report the synthesis of various additional polyamines conjugated to green fluorophore headgroups. First, BODIPY-FL-T-polyamines were synthesized *via* a similar click-chemistry reaction as for the original BODIPY probes [21], but with the difference that azido-polyamines (-PUT, -SPD or -SPM) were clicked onto the alkyne-BODIPY-FL fluorophore. This resulted in the formation of a triazole ring (T) between the polyamine and the BODIPY-FL groups (referred to as FL-T probe, **compounds 2a-c**, **Figure 4**). Second, a succinimidyl ester–amine coupling strategy yielded the synthesis of BODIPY-FL-A conjugated polyamines in which an amide bond (A) is created between the polyamine and BODIPY-FL groups (referred to as FL-A probe, **compounds 3a-c**, **Figure 4**). Lastly, an isothiocyanate–amine coupling strategy was used to generate FITC-conjugated polyamines with a thiourea bond between the polyamine and the fluorophore (referred as FITC probes, **compounds 4a-c**, **Figure 4**). The detailed chemical synthesis of each polyamine-conjugate is outlined in **Supplementary Information** and the complete chemical structures are drawn in **Figure S4A-C**. As expected, the fluorescent properties of the different fluorophore-polyamine conjugates (i.e. the wavelengths of maximum absorption and emission λ_{Abs} (max) and λ_{Em} (max) as well as the Stokes' shift) are very similar (**Figure S4E**).

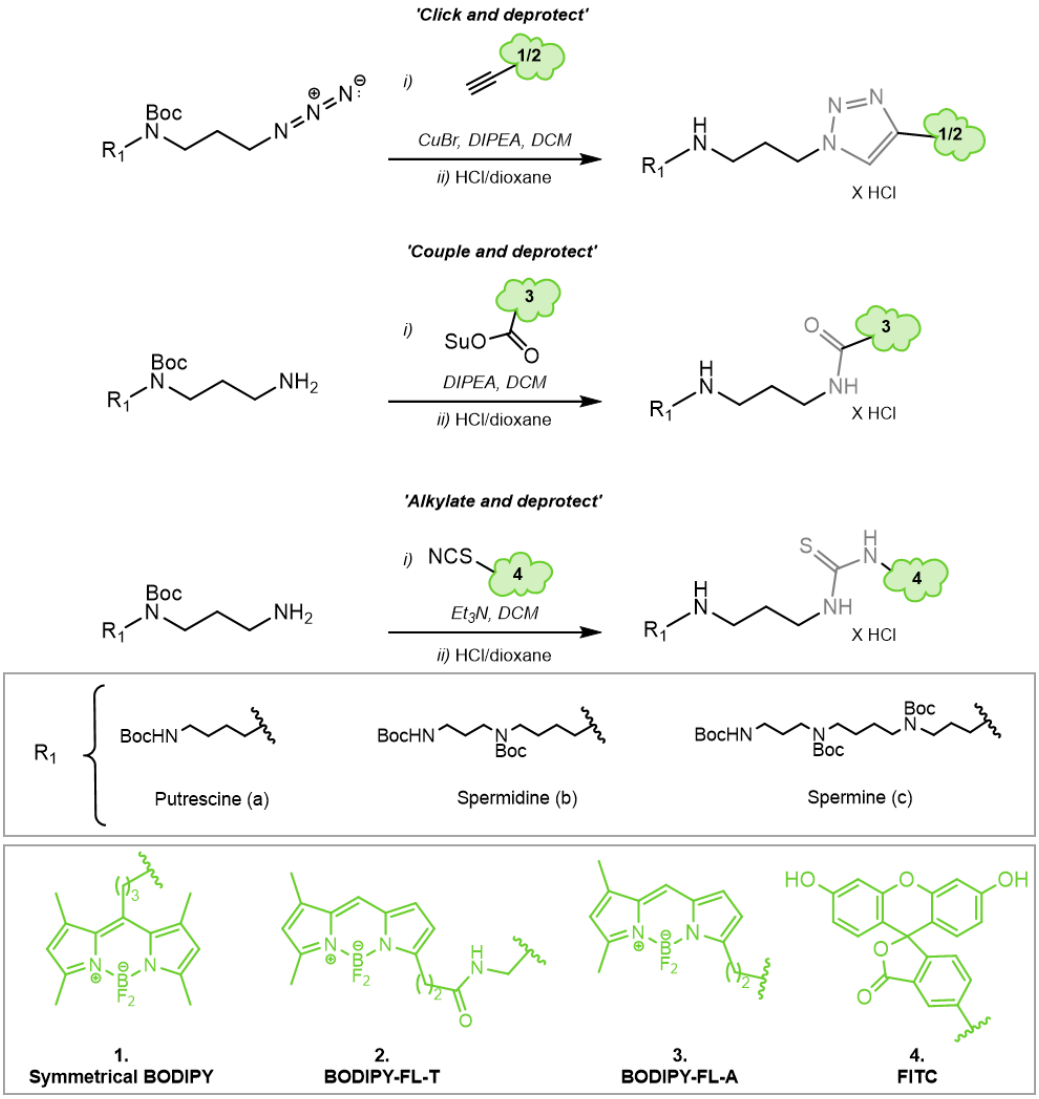

Figure 4. Simplified scheme representing the chemical synthesis of the different green fluorescent polyamine conjugates used in the study. A detailed description of the synthesis is given in **Supplementary Information**.

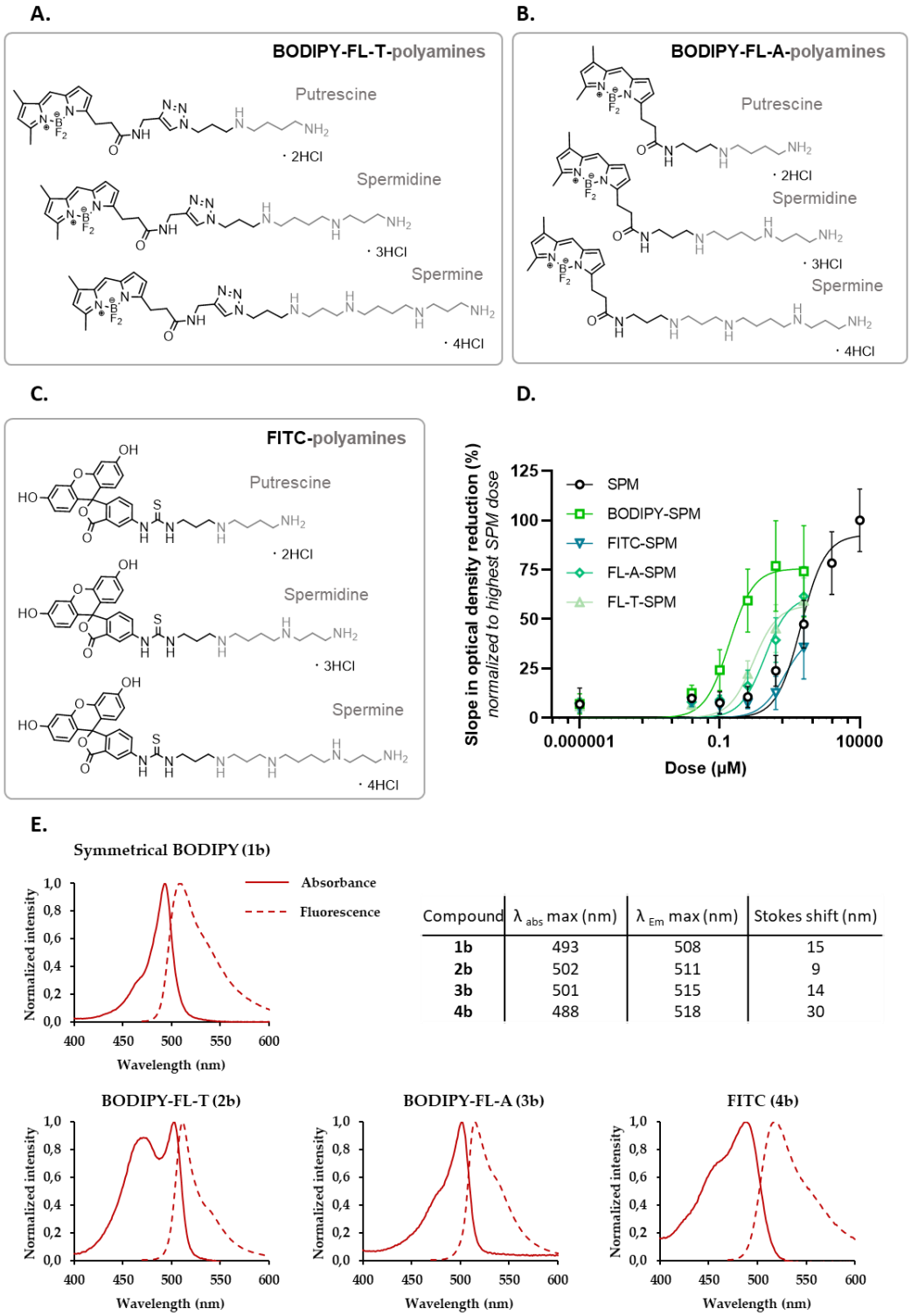

Compound	λ_{abs} max (nm)	λ_{Em} max (nm)	Stokes shift (nm)
1b	493	508	15
2b	502	511	9
3b	501	515	14
4b	488	518	30

Figure S4. Full structures of the different green fluorescent polyamine conjugates used in the study and biochemical characterization of spermine conjugates. **A.** FL-T-polyamine structures. **B**. FL-T-polyamine structures. **C**. FITC-polyamine structures. **D**. ATP/NADH-enzyme coupled ATPase assay. ATPase activity of purified ATP13A2 (1.25 µg) measured in the presence of increasing concentration of the following substrates: unlabeled spermine (SPM), BODIPY-SPM, FITC-SPM, FL-A-SPM and FL-T-SPM (N=3 to 9, technical duplicates). The Y axis depicts the slope in optical density at 340 nm reflecting NADH consumption and further

ATP consumption, normalized to the highest dose of SPM. **E**. Normalized absorption and emission spectra of symmetrical BODIPY-SPD (1b), BODIPY-FL-T-SPD (2b), BODIPY-FL-A-SPD (3B) and FITC-SPD (4b) together with a table providing the spectral properties of these compounds.

To evaluate whether the new probes are substrates for ATP13A2, we performed ATP/NADH enzyme-coupled ATPase assays on purified ATP13A2 with FL-A-SPM, FL-T-SPM and FITC-SPM (**Figure S4D**) using SPM and BODIPY-SPM as references. ATP13A2's activity is not only stimulated by SPM and BODIPY-SPM, but also by FL-A-, FL-T- and FITC-SPM showing that the different fluorophores or coupling strategies do not prevent the recognition of the polyamine core as a substrate. Interestingly, only BODIPY-SPM, but not the other fluorophore-SPM conjugates display a higher apparent affinity for ATP13A2, since the new probes stimulate ATP13A2 ATPase activity to the same extent as the unlabeled SPM up to a concentration of 10 µM (**Figure S4D**).

4. Fluorescent polyamine probes present different structure-function relationships towards ATP13A2 and ATP13A3.

In a next step, we compared the uptake of the new green fluorescent polyamines in both ATP13A2 and ATP13A3 cell models using the original BODIPY-polyamines as a reference (**Figure 5A, E**). ATP13A3 and ATP13A2 cell models were exposed to a fixed concentration of 5 µM fluorescent polyamine for 30 min or 2 h, respectively (**Figure 5**). In general, we observed a larger fold-change of uptake with the new FL-A and FL-T probes than with the reference BODIPY polyamines. The large window between uptake in cells expressing WT *versus* the catalytic dead mutant shows that all probes are mainly transported *via* the catalytic activity of ATP13A2 or ATP13A3 (**Figure 5**), in line with the ATPase data for ATP13A2 (**Figure 4**). Strikingly, the uptake windows obtained with the new BODIPY-FL-probes (FL-A and FL-T) are much larger than with the reference BODIPY polyamines. The structural difference lies not only in the substitution pattern on the fluorophore core, but also on the position of the connection towards the polyamine. Both of these factors may affect the cellular uptake *via* ATP13A2 and/or ATP13A3. Despite their lower apparent affinity for the transporter compared with the original BODIPY analogs, the signal to noise ratio for the uptake was highest with the FL-A probes, followed by the FL-T probes.

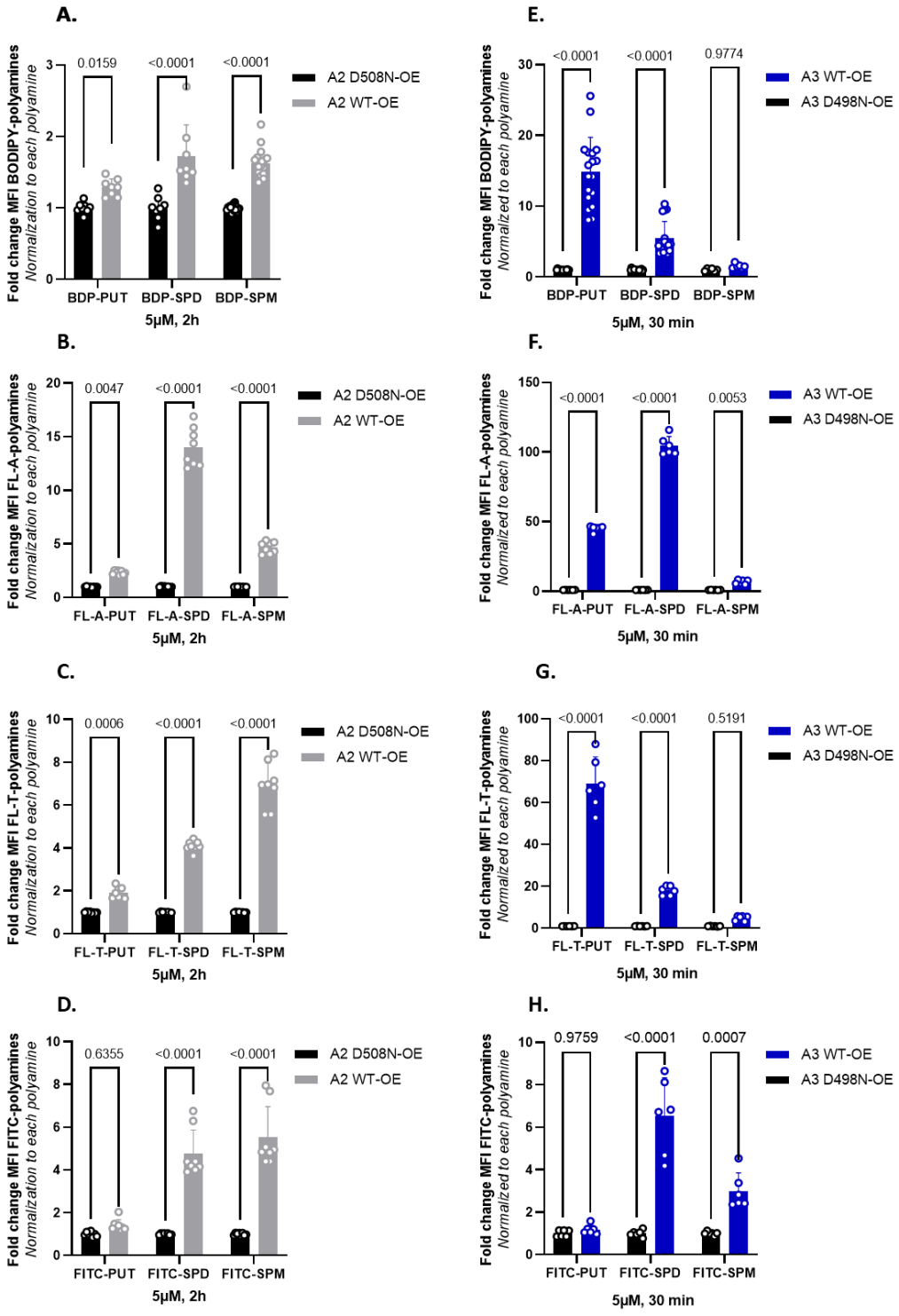

Figure 5. Comparison of the cellular uptake of BODIPY-conjugated *versus* BODIPY-FL-A, BODIPY-FL-T and FITC-conjugated polyamines in ATP13A2 and ATP13A3 cell models. A.-D. SH-SY5Y ATP13A2 WT-OE and D508N-OE cells were incubated for 2 h with 5 µM of each fluorescently labeled polyamine. **E.-H.** HMEC-1 ATP13A3 WT-OE and D498N-OE cells were incubated for 30 min with 5 µM of each fluorescently labeled polyamine. The mean fluorescence intensity (MFI) was recorded using a BD Canto II flow cytometer based on the settings used for BODIPY-polyamines and normalized as indicated on the Y axis. Experiments were done four independent times (N=4) in ATP13A2 cell model and three independent times (N=3) in ATP13A3 cell model,

with technical duplicates. Statistical analysis was done using GraphPad Prism and a two-way ANOVA test with Sidak's multiple comparison test.

In line with the biochemically confirmed substrate specificity, A2 WT-OE cells present a significantly higher uptake of all SPD and SPM conjugates. A more modest, but significant uptake of the BODIPY-PUT analogs was observed, whereas uptake of FITC-PUT was not significantly different from A2 D508N-OE cells (**Figure 5D, H**). Conversely, A3 WT-OE cells exhibit a higher uptake of BODIPY-labeled PUT and SPD probes than of the fluorescent SPM conjugates (significantly different only for FITC-SPM and FL-A-SPM). The fluorophore FITC seems to prevent PUT recognition in ATP13A3 cells (**Figure 5H**). This is remarkable, because ATP13A3 accepts all other fluorophore-PUT conjugates reported here (**Figure 3E-F**, **Figure 5E-G**), as well as ^{14}C-PUT (**Figure 3E, F**). Notably, FL-A-SPD offers the best uptake window for both ATP13A2 (14-fold) or ATP13A3 (105-fold), and therefore emerges as the best probe to follow either ATP13A2 or ATP13A3 transport activity in cells. Conversely, FL-T-PUT exhibits the highest specificity for ATP13A3 (35-fold more uptake in ATP13A3 *versus* ATP13A2 cells), whereas FITC-SPM presents the highest specificity for ATP13A2 (1.8-fold more uptake in ATP13A2 *versus* ATP13A3 cells). Together, our data show that ATP13A2 and ATP13A3 exhibit overlap in substrate specificity, whereas a probe specific structure-activity relationship (SAR) towards ATP13A2 and ATP13A3 has been observed (**Figure 5F, G**).

Discussion

Fluorescently labeled polyamine conjugates represent powerful tools to assess polyamine transport at the cellular level and dissect the mPTS that remains poorly characterized. In this study, we compared the properties of different green fluorescently labeled polyamines to analyze the transport activity in cells of the two housekeeping P_{5B}-type ATPases, ATP13A2 and ATP13A3, which emerge as major determinants of cellular polyamine uptake [11,13].

1. Comparison of ATP13A2 and ATP13A3 substrate specificity

We provided the first biochemical evidence that fluorescently labeled polyamines stimulate the catalytic turnover of ATP13A2 indicating that they are genuine substrates of ATP13A2. We previously documented that fluorescent polyamine conjugates enter cells *via* endocytosis [13] and are subsequently transported *via* the activity of ATP13A2 from late endo/lysosomes to the cytosol and further into other compartments, including mitochondria [13,23]. We also showed that ATP13A2 activity responds to a range of fluorescent polyamine analogs indicating flexibility of the substrate binding pocket. We observed the best correlation between the cellular uptake levels of BODIPY-FL-T labeled polyamines (BODIPY-FL-T SPM > SPD > PUT) and the reported apparent affinity of ATP13A2 for unlabeled polyamines (SPM > SPD > PUT; [13]). This correlation is weaker for other polyamine conjugates, indicating that BODIPY-FL-T probes may accommodate best to the substrate binding pockets amongst the here tested fluorophore polyamine analogs.

The radio- and fluorescently-labeled polyamine uptake data for ATP13A3 point to PUT and SPD as preferred substrates of the protein, but not all polyamine probes provide the same results. All fluorescent SPD analogs and the radiolabeled SPD probe are taken up *via* ATP13A3, indicating that SPD truly represents a transported substrate. ATP13A3 also promotes the uptake of radiolabeled PUT, which is in line with the strong uptake of PUT coupled to BODIPY, BODIPY-FL-A or BODIPY-FL-T. These data are in good agreement with our previous study in CHO-MG cells where ATP13A3 complements PUT uptake deficiency [11]. However, no ATP13A3-dependent uptake was observed with FITC-PUT suggesting that the FITC-label disrupts PUT recognition by ATP13A3. Conversely, only FITC-SPM, but not other SPM analogs, are taken up in cells *via* ATP13A3, making it less likely that SPM represents a transported substrate of ATP13A3. This contrasts with a recent study that highlighted both SPD and

SPM, but not PUT, as likely ATP13A3 substrates based on radiolabeled uptake experiments in pancreatic cancer cells [15]. On the other hand, in CHO-MG cell models, we previously observed that unlabeled PUT, SPD and SPM competed with BODIPY–PUT uptake *via* ATP13A3, indicating that PUT, SPD and SPM may all be transported by ATP13A3 [11]. The apparent discrepancy between these studies may point to cell-type specific properties of ATP13A3 or may reflect differences in the experimental conditions, such as exposure time, fluorescent polyamine concentrations or cell culture conditions. Based on the uptake data it remains challenging to pinpoint the precise endogenous substrates of ATP13A3, and biochemical confirmation on purified ATP13A3 will be required to establish the relative affinities of ATP13A3 towards the endogenous polyamine species.

The overlapping substrate specificities suggest that ATP13A2 and ATP13A3 fulfill - at least in part - redundant functions in cellular polyamine uptake. This has been confirmed in CHO-MG cells with loss of ATP13A3 functionality that can be fully rescued not only with ATP13A3, but also with ATP13A2 complementation [11]. It remains unclear whether the redundancy of the isoforms would play a compensatory or maladaptive role in diseases associated with ATP13A2 or ATP13A3 mutations.

Overall, our series of green fluorescent probes are useful tools to assess ATP13A2 and ATP13A3 activity in cells, but not to deduce the endogenous substrate specificities. While both isoforms promote the uptake of all SPD labeled analogs, FL-A-SPD offers the best uptake window. FL-A-SPD therefore emerges as an excellent probe to follow the combined cellular activity of ATP13A2 and ATP13A3 with high sensitivity and uptake potential.

2. Towards the design of ATP13A2 and ATP13A3 specific polyamine probes

ATP13A2 and ATP13A3 both transport SPD pointing to an overlap in substrate specificity. However, the P_{5B} isoforms present differences in their activity towards PUT or SPM analogs, since the fluorophore and coupling strategies differently affect the uptake of the probes in ATP13A2 *versus* ATP13A3 cell models. So far, FL-T-PUT emerges as the best polyamine analog to probe ATP13A3 activity selectively, whereas FITC-SPM may be considered to more selectively follow ATP13A2 activity. Previously, we described that ATP13A3, but not ATP13A2, mediates cellular toxicity to methylglyoxal bis-(guanylhydrazone) (MGBG), a toxic SPD analog and an inhibitor of polyamine biosynthesis [11]. The

overlapping, as well as isoform–specific substrate recognition of ATP13A2 *versus* ATP13A3 is compatible with a strong, but not complete, conservation of the substrate binding pocket between P_{5B} isoforms. Indeed, most critical residues for polyamine binding and recognition are conserved between ATP13A2 and ATP13A3 [19], allowing that the polyamine part of the fluorescent probe may enter the channel-like polyamine binding pocket regardless of the linker or fluorophore. Polyamines bind in their linear form and the polyamine affinity depends on the number of amine groups and the spacing between them [19]. The polyamine part of the fluorescent probes may subsequently translocate within the membrane domain of the transporter following an unresolved path. Since the polyamine binding site may be too narrow to accommodate a bulky fluorescent headgroup, we hypothesize that the fluorescent tag may instead move along/in between transmembrane helices or – given its hydrophobic nature- may stick out within the membrane bilayer. The translocation mechanism of fluorescent polyamines may resemble the 'credit card swipe' mechanism described in lipid flippases of the P_4-type ATPase family. An entire phospholipid substrate does not fit within the central transmembrane domain of the flippase, hence only the polar headgroup region of the phospholipid interacts with the protein, while the fatty acyl tails slide through the hydrophobic region of the lipid bilayer membrane surrounding the protein [28]. A similar translocation mechanism for the fluorescently labeled polyamines may explain why ATP13A2 and ATP13A3 translocate fluorescent polyamine analogs with different fluorophores and linkers. The isoform-specific amino-acid differences in the proximity of the polyamine binding site may contribute to the SAR by influencing the passage of the bulky fluorescent label. The higher apparent affinity of ATP13A2 for BODIPY-SPM as compared to SPM or other fluorescent SPM probes may therefore be possibly explained by specific interactions between BODIPY and surrounding residues in the transmembrane domain. Besides BODIPY- and FITC-labeled polyamines, also nitrobenzoxadiazolyl (NBD)- [29], antracene- [30] and indotricarbocyanine-labeled polyamines [31] have previously been developed to monitor the activity of the mPTS. Also the NBD-labeled spermine is most likely taken up *via* ATP13A3 [15], but it remains to be tested whether all these probes are indeed transported *via* ATP13A2 and/or ATP13A3.

3. Distinct polyamine uptake kinetics in ATP13A2 and ATP13A3 cells

Although cell type specific differences may play a role, we found that ATP13A3 mediates stronger and faster uptake of radio- and fluorescently labeled polyamines than ATP13A2. ATP13A3 contributes much more to cellular PUT and SPD uptake than ATP13A2. ATP13A3 may also contribute more to cellular SPM uptake, since the uptake of fluorescent SPM analogs in ATP13A2 and ATP13A3 cells is comparable despite the shorter treatment time in ATP13A3 models. The expression of ATP13A3 in earlier compartments of the endosomal system as well as specific biochemical properties (K_m ,V_{max}) may explain the more dominant and faster polyamine uptake via ATP13A3 over ATP13A2.

Our results show that with a proper choice of the polyamine probe, concentration and short treatment time, it is possible to exclusively measure ATP13A3 dependent uptake in cells expressing both ATP13A2 and ATP13A3. However, it remains much more challenging to dissect the ATP13A2 activity in the background of ATP13A3, since ATP13A2-specific probes have not yet been identified. In addition, endocytosed probes first meet ATP13A3 in the earlier endosomal compartments from which they can be exported by ATP13A3 before reaching ATP13A2 in the late endo/lysosomal compartments.

Importantly, the distinct substrate specificities and uptake kinetics of ATP13A2 as well as the contribution of the fluorophore and linker to substrate recognition and affinity indicate that designing ATP13A2-specific probes may be feasible. With isoform specific probes we would be able to follow transporter specific uptake in various cell types and physiological conditions. In disease models we may pick up isoform-specific transport deficiencies and map possible compensatory changes in the activity of other P_{5B} ATPase isoforms. Moreover, the broad range of fluorescent polyamines that enter cells *via* ATP13A2 and/or ATP13A3, suggest that polyamines may be considered as vehicles to take up drugs or other molecular cargo [32]. For instance, polyamine-antracene conjugates have previously been designed to target cancer cells with an increased polyamine uptake system [33] or *Plasmodium falciparum* parasites [34]. Structural studies of P_{5B}-ATPases with bound polyamine conjugates as well as functional analysis of other polyamine conjugates will lead to a better understanding of the SAR, which will facilitate the design of isoform-specific strategies.

4. Green fluorescent probes with improved synthesis and properties

The novel green fluorescent polyamine probes described here follow two different synthetic strategies. Our original synthesis encompassed a click chemistry-based approach between an azide-functionalized polyamine and an alkyne-labeled BODIPY fluorophore. Here, we also explored amide and isothiocyanate coupling to a properly protected polyamine analog with one single free amino group. Conveniently, such protected polyamines are intermediates in our original probe synthesis, and therefore shorten the route by one step. We found that the amide coupling strategy gave rise to the most promising fluorescent polyamine series (BODIPY-FL-A series; **3a-c**). As many more fluorophore oxysuccinimide esters are available from commercial sources, we expect that other analogs can be readily synthesized, opening the way to further improvement of the fluorescent polyamine properties.

Here, we found that the new probes, despite having a lower affinity than our previously reported fluorescent polyamine probes, display a higher cellular uptake at 5 µM. It indicates that the new probes (except for FITC-PUT, **4c**) are superior substrates for ATP13A2 and ATP13A3, and underlines the importance of the nature of the fluorophore and the coupling strategy between the fluorophore and the polyamine.

In conclusion, the here reported fluorescent polyamine probes are attractive for the study of polyamine uptake by ATP13A2 and APT13A3, and the BODIPY-FL-A series emerged as the most efficient of the tools described here.

Author Contributions: "Conceptualization, P.V. and S.V.; methodology, M.H., N.J., J.C., M.A. and C.VdH; validation, M.H., N.J. and J.C.; formal analysis, M.H.; resources, C.VdH, J.C., R.V. and S.V.; data curation, N.J., J.C. and M.H.; writing—original draft preparation, M.H. and P.V.; writing—review and editing, M.H., N.J., J.C., S.V., V.D., J.E. and P.V.; supervision, M.H., P.V. and S.V.; project administration, V.D.; funding acquisition, P.V., V.D. and S.V.. All authors have read and agreed to the published version of the manuscript."

Funding: This research was funded by the C3/20/035 grant of KU Leuven allocated to V.D., S.V. and P.V. and the Aligning Science Across Parkinson's [ASAP-000458] through the Michael J. Fox

Foundation for Parkinson's Research (MJFF) allocated to P.V.. For the purpose of open access, the author has applied a CC BY license (https://creativecommons.org/licenses/by/4.0/). M.A. is an aspirant research fellow of the Fonds voor Wetenschappelijk Onderzoek (FWO) - Flanders (1S77920N).

Supplementary Materials: Figure *S*1: Characterization of ATP13A2-expressing SH-SY5Y cell models; Figure S2: Characterization of ATP13A3-expressing HMEC-1 cell models; Figure S3: BODIPY-PUT and BODIPY-SPD uptake in HMEC-1 cells overexpressing ATP13A3 WT or D498N; Figure *S*4. Full structures of the different green fluorescent polyamine conjugates used in the study and biochemical characterization of spermine conjugates; Figure S5: Synthesis of putrescine precursors, reagents and conditions; Figure S6: Synthesis of spermine and spermidine precursors, reagents and conditions; Figure S7: Conjugation of the fluorophore to the relevant protected polyamine; Figure S8: Boc-deprotection of the relevant Boc-protected probe; as well as detailed synthesis procedures, ^{1}H-NMR, ^{13}C-NMR, HRMS and LC-purity data.

Data Availability Statement: All datasets generated or analyzed in this study can be found through the Zenodo depository, reserved doi: 10.5281/zenodo.7434965. All experimental protocols can be found on protocols.io.

Acknowledgments: We would like to thank Marleen Schuermans and Marijke De Jaeger for technical support; Luc Baudemprez for collecting the NMR data data and Dr Eduard Fron for acquiring absorption and emission spectra of the probes. HRMS was made possible by the support of the Hercules Foundation of the Flemish Government (grant 20100225–7). We also acknowledge our frequent use of the facilities and equipment of the Leuven Viral Vector Core facility (KU Leuven) and the FACS Core (KU Leuven/VIB).

Conflicts of Interest: The authors declare no conflict of interest. KU Leuven has granted EMD Millipore Corporation an exclusive license for the commercialization of BODIPY-PUT, BODIPY-SPD and BODIPY-SPM described in this study.

References

1. Minois, N.; Carmona-Gutierrez, D.; Madeo, F. Polyamines in aging and disease. *Aging (Albany NY)* **2011**, *3*, 716-732, doi:10.18632/aging.100361.

2. Pegg, A.E. Mammalian polyamine metabolism and function. *IUBMB Life* **2009**, *61*, 880-894, doi:10.1002/iub.230.

3. Eisenberg, T.; Abdellatif, M.; Schroeder, S.; Primessnig, U.; Stekovic, S.; Pendl, T.; Harger, A.; Schipke, J.; Zimmermann, A.; Schmidt, A.; et al. Cardioprotection and lifespan extension by the natural polyamine spermidine. *Nat Med* **2016**, *22*, 1428-1438, doi:10.1038/nm.4222.

4. Eisenberg, T.; Knauer, H.; Schauer, A.; Buttner, S.; Ruckenstuhl, C.; Carmona-Gutierrez, D.; Ring, J.; Schroeder, S.; Magnes, C.; Antonacci, L.; et al. Induction of autophagy by spermidine promotes longevity. *Nat Cell Biol* **2009**, *11*, 1305-1314, doi:10.1038/ncb1975.

5. Poulin, R.; Casero, R.A.; Soulet, D. Recent advances in the molecular biology of metazoan polyamine transport. *Amino Acids* **2012**, *42*, 711-723, doi:10.1007/s00726-011-0987-y.

6. Belting, M.; Mani, K.; Jonsson, M.; Cheng, F.; Sandgren, S.; Jonsson, S.; Ding, K.; Delcros, J.G.; Fransson, L.A. Glypican-1 is a vehicle for polyamine uptake in mammalian cells: a pivital role for nitrosothiol-derived nitric oxide. *J Biol Chem* **2003**, *278*, 47181-47189, doi:10.1074/jbc.M308325200.

7. Cheng, F.; Fransson, L.A.; Mani, K. Common traffic routes for imported spermine and endosomal glypican-1-derived heparan sulfate in fibroblasts. *Exp Cell Res* **2018**, *364*, 133-142, doi:10.1016/j.yexcr.2018.01.029.

8. Palmer, A.J.; Wallace, H.M. The polyamine transport system as a target for anticancer drug development. *Amino Acids* **2010**, *38*, 415-422, doi:10.1007/s00726-009-0400-2.

9. Soulet, D.; Gagnon, B.; Rivest, S.; Audette, M.; Poulin, R. A fluorescent probe of polyamine transport accumulates into intracellular acidic vesicles via a two-step mechanism. *J Biol Chem* **2004**, *279*, 49355-49366, doi:10.1074/jbc.M401287200.

10. Uemura, T.; Stringer, D.E.; Blohm-Mangone, K.A.; Gerner, E.W. Polyamine transport is mediated by both endocytic and solute carrier transport mechanisms in the gastrointestinal tract. *Am J Physiol Gastrointest Liver Physiol* **2010**, *299*, G517-522, doi:10.1152/ajpgi.00169.2010.

11. Hamouda, N.N.; Van den Haute, C.; Vanhoutte, R.; Sannerud, R.; Azfar, M.; Mayer, R.; Cortes Calabuig, A.; Swinnen, J.V.; Agostinis, P.; Baekelandt, V.; et al. ATP13A3 is a major component of the enigmatic mammalian polyamine transport system. *J Biol Chem* **2021**, *296*, 100182, doi:10.1074/jbc.RA120.013908.

12. Sorensen, D.M.; Holemans, T.; van Veen, S.; Martin, S.; Arslan, T.; Haagendahl, I.W.; Holen, H.W.; Hamouda, N.N.; Eggermont, J.; Palmgren, M.; et al. Parkinson disease related ATP13A2 evolved early in animal evolution. *PLoS One* **2018**, *13*, e0193228, doi:10.1371/journal.pone.0193228.

13. van Veen, S.; Martin, S.; Van den Haute, C.; Benoy, V.; Lyons, J.; Vanhoutte, R.; Kahler, J.P.; Decuypere, J.P.; Gelders, G.; Lambie, E.; et al. ATP13A2 deficiency disrupts lysosomal polyamine export. *Nature* **2020**, *578*, 419-424, doi:10.1038/s41586-020-1968-7.

14. Azfar, M.; van Veen, S.; Houdou, M.; Hamouda, N.N.; Eggermont, J.; Vangheluwe, P. P5B-ATPases in the mammalian polyamine transport system and their role in disease. *Biochim Biophys Acta Mol Cell Res* **2022**, *1869*, 119354, doi:10.1016/j.bbamcr.2022.119354.

15. Sekhar, V.; Andl, T.; Phanstiel, O.t. ATP13A3 facilitates polyamine transport in human pancreatic cancer cells. *Sci Rep* **2022**, *12*, 4045, doi:10.1038/s41598-022-07712-4.

16. Chen, X.; Zhou, M.; Zhang, S.; Yin, J.; Zhang, P.; Xuan, X.; Wang, P.; Liu, Z.; Zhou, B.; Yang, M. Cryo-EM structures and transport mechanism of human P5B type ATPase ATP13A2. *Cell Discov* **2021**, *7*, 106, doi:10.1038/s41421-021-00334-6.

17. Li, P.; Wang, K.; Salustros, N.; Gronberg, C.; Gourdon, P. Structure and transport mechanism of P5B-ATPases. *Nat Commun* **2021**, *12*, 3973, doi:10.1038/s41467-021-24148-y.

18. Sim, S.I.; von Bulow, S.; Hummer, G.; Park, E. Structural basis of polyamine transport by human ATP13A2 (PARK9). *Mol Cell* **2021**, *81*, 4635-4649 e4638, doi:10.1016/j.molcel.2021.08.017.

19. Tillinghast, J.; Drury, S.; Bowser, D.; Benn, A.; Lee, K.P.K. Structural mechanisms for gating and ion selectivity of the human polyamine transporter ATP13A2. *Mol Cell* **2021**, *81*, 4650-4662 e4654, doi:10.1016/j.molcel.2021.10.002.

20. Tomita, A.; Daiho, T.; Kusakizako, T.; Yamashita, K.; Ogasawara, S.; Murata, T.; Nishizawa, T.; Nureki, O. Cryo-EM reveals mechanistic insights into lipid-facilitated polyamine export by human ATP13A2. *Mol Cell* **2021**, *81*, 4799-4809 e4795, doi:10.1016/j.molcel.2021.11.001.

21. Vanhoutte, R.; Kahler, J.P.; Martin, S.; van Veen, S.; Verhelst, S.H.L. Clickable Polyamine Derivatives as Chemical Probes for the Polyamine Transport System. *Chembiochem* **2018**, *19*, 907-911, doi:10.1002/cbic.201800043.

22. Mandel, J.L.; Flintoff, W.F. Isolation of mutant mammalian cells altered in polyamine transport. *J Cell Physiol* **1978**, *97*, 335-343, doi:10.1002/jcp.1040970308.

23. Vrijsen, S.; Besora-Casals, L.; van Veen, S.; Zielich, J.; Van den Haute, C.; Hamouda, N.N.; Fischer, C.; Ghesquiere, B.; Tournev, I.; Agostinis, P.; et al. ATP13A2-mediated endo-lysosomal

polyamine export counters mitochondrial oxidative stress. *Proc Natl Acad Sci U S A* **2020**, *117*, 31198-31207, doi:10.1073/pnas.1922342117.

24. Barozzi, C.; Galletti, M.; Tomasi, L.; De Fanti, S.; Palazzini, M.; Manes, A.; Sazzini, M.; Galie, N. A Combined Targeted and Whole Exome Sequencing Approach Identified Novel Candidate Genes Involved in Heritable Pulmonary Arterial Hypertension. *Sci Rep* **2019**, *9*, 753, doi:10.1038/s41598-018-37277-0.

25. Graf, S.; Haimel, M.; Bleda, M.; Hadinnapola, C.; Southgate, L.; Li, W.; Hodgson, J.; Liu, B.; Salmon, R.M.; Southwood, M.; et al. Identification of rare sequence variation underlying heritable pulmonary arterial hypertension. *Nat Commun* **2018**, *9*, 1416, doi:10.1038/s41467-018-03672-4.

26. Machado, R.D.; Welch, C.L.; Haimel, M.; Bleda, M.; Colglazier, E.; Coulson, J.D.; Debeljak, M.; Ekstein, J.; Fineman, J.R.; Golden, W.C.; et al. Biallelic variants of ATP13A3 cause dose-dependent childhood-onset pulmonary arterial hypertension characterised by extreme morbidity and mortality. *J Med Genet* **2022**, *59*, 906-911, doi:10.1136/jmedgenet-2021-107831.

27. Morrell, N.W.; Aldred, M.A.; Chung, W.K.; Elliott, C.G.; Nichols, W.C.; Soubrier, F.; Trembath, R.C.; Loyd, J.E. Genetics and genomics of pulmonary arterial hypertension. *Eur Respir J* **2019**, *53*, doi:10.1183/13993003.01899-2018.

28. Shukla, S.; Baumgart, T. Enzymatic trans-bilayer lipid transport: Mechanisms, efficiencies, slippage, and membrane curvature. *Biochim Biophys Acta Biomembr* **2021**, *1863*, 183534, doi:10.1016/j.bbamem.2020.183534.

29. Guminski, Y.; Grousseaud, M.; Cugnasse, S.; Brel, V.; Annereau, J.P.; Vispe, S.; Guilbaud, N.; Barret, J.M.; Bailly, C.; Imbert, T. Synthesis of conjugated spermine derivatives with 7-nitrobenzoxadiazole (NBD), rhodamine and bodipy as new fluorescent probes for the polyamine transport system. *Bioorg Med Chem Lett* **2009**, *19*, 2474-2477, doi:10.1016/j.bmcl.2009.03.052.

30. Wang, C.; Delcros, J.G.; Cannon, L.; Konate, F.; Carias, H.; Biggerstaff, J.; Gardner, R.A.; Phanstiel, I.V.O.t. Defining the molecular requirements for the selective delivery of polyamine conjugates into cells containing active polyamine transporters. *J Med Chem* **2003**, *46*, 5129-5138, doi:10.1021/jm030223a.

31. Konig, S.G.; Oz, S.; Kramer, R. A polyamine-modified near-infrared fluorescent probe for selective staining of live cancer cells. *Chem Commun (Camb)* **2015**, *51*, 7360-7363, doi:10.1039/c5cc01637a.

32. Nazifi, S.M.R.; Sadeghi-aliabadi, H.; Fassihi, A.; Saghaie, L. Structure–activity relationship of polyamine conjugates for uptake via polyamine transport system. *Structural Chemistry* **2019**, *30*, 175-184, doi:https://doi.org/10.1007/s11224-018-1175-4.

33. Traquete, R.; Ghani, R.A.; Phanstiel, O.; Wallace, H.M. Ant 4,4, a polyamine-anthracene conjugate, induces cell death and recovery in human promyelogenous leukemia cells (HL-60). *Amino Acids* **2013**, *44*, 1193-1203, doi:10.1007/s00726-012-1452-2.

34. Niemand, J.; Burger, P.; Verlinden, B.K.; Reader, J.; Joubert, A.M.; Kaiser, A.; Louw, A.I.; Kirk, K.; Phanstiel, O.t.; Birkholtz, L.M. Anthracene-polyamine conjugates inhibit in vitro proliferation of intraerythrocytic Plasmodium falciparum parasites. *Antimicrob Agents Chemother* **2013**, *57*, 2874-2877, doi:10.1128/AAC.00106-13.

References used in Supplementary information

[11, 21]